INTERFACE

rsif.royalsocietypublishing.org

Research

Cite this article: Li X, Liu X, Zhang P, Feng C, Sun A, Kang H, Deng X, Fan Y. 2017 Numerical simulation of haemodynamics and low-density lipoprotein transport in the rabbit aorta and their correlation with atherosclerotic plaque thickness. *J. R. Soc. Interface* **14**: 20170140. http://dx.doi.org/10.1098/rsif.2017.0140

Received: 27 February 2017
Accepted: 20 March 2017

Subject Category:
Life Sciences–Engineering interface

Subject Areas:
bioengineering, biomedical engineering, biomechanics

Keywords:
atherosclerosis, wall shear stress, low-density lipoproteins, concentration polarization, lipid deposition

Authors for correspondence:
Xiaoyan Deng
e-mail: dengxy1953@buaa.edu.cn
Yubo Fan
e-mail: yubofan@buaa.edu.cn

†These authors contributed equally to this study.

THE ROYAL SOCIETY PUBLISHING

Numerical simulation of haemodynamics and low-density lipoprotein transport in the rabbit aorta and their correlation with atherosclerotic plaque thickness

Xiaoyin Li[1,†], Xiao Liu[1,†], Peng Zhang[1], Chenglong Feng[1], Anqiang Sun[1], Hongyan Kang[1], Xiaoyan Deng[1] and Yubo Fan[1,2]

[1]Key Laboratory for Biomechanics and Mechanobiology of the Ministry of Education, School of Biological Science and Medical Engineering, Beihang University, Beijing 100191, People's Republic of China
[2]National Research Center for Rehabilitation Technical Aids, Beijing, People's Republic of China

XL, 0000-0001-7935-2444

Two mechanisms of shear stress and mass transport have been recognized to play an important role in the development of localized atherosclerosis. However, their relationship and roles in atherogenesis are still obscure. It is necessary to investigate quantitatively the correlation among low-density lipoproteins (LDL) transport, haemodynamic parameters and plaque thickness. We simulated blood flow and LDL transport in rabbit aorta using computational fluid dynamics and evaluated plaque thickness in the aorta of a high-fat-diet rabbit. The numerical results show that regions with high luminal LDL concentration tend to have severely negative haemodynamic environments (HEs). However, for regions with moderately and slightly high luminal LDL concentration, the relationship between LDL concentration and the above haemodynamic indicators is not clear cut. Point-by-point correlation with experimental results indicates that severe atherosclerotic plaque corresponds to high LDL concentration and seriously negative HEs, less severe atherosclerotic plaque is related to either moderately high LDL concentration or moderately negative HEs, and there is almost no atherosclerotic plaque in regions with both low LDL concentration and positive HEs. In conclusion, LDL distribution is closely linked to blood flow transport, and the synergetic effects of luminal surface LDL concentration and wall shear stress-based haemodynamic indicators may determine plaque thickness.

1. Introduction

It is well documented that atherosclerosis is much more prone to occurring in particular regions of the arterial system where the geometry changes sharply, such as arterial branching, curvature and vascular stenosis, which is referred to the localization of atherosclerosis [1,2]. Two mechanisms have been proposed to explain the phenomenon [3]. One is the vascular responses to abnormal blood flow-induced shear stress [4–6]. The other one is the localized alterations in mass transport [4,7–15]. For the shear stress mechanism, it is believed that the blood flow in these predisposed areas is disturbed, which would directly affect the phenotype of endothelial cells by regulating some atherogenic genes and proteins and hence promote the development of atherosclerosis [16–18]. To quantify the disturbed blood flow in these regions, several haemodynamic indicators have been introduced. The first one is wall shear stress (WSS) which is the frictional force induced by the movement of blood flow on the endothelial cell [4]. High WSS would protect the artery, while low WSS (less than 4 dyne cm^{-2}) would stimulate an atherogenic phenotype of endothelial cells [5]. In addition to WSS, other haemodynamic parameters

based on WSS were also deemed to have a close relationship with atherosclerosis. For instance, high oscillating shear index (OSI) and relative residence time (RRT) could promote the occurrence and development of atherosclerosis [19,20]. Recently, researchers proposed that the high value of transverse wall shear stress (transWSS), describing multi-directionality of blood flow, may also be important in the occurrence of atherosclerosis [21,22].

Nevertheless, the accumulation of lipids within the arterial wall is considered to be the key factor of the initial genesis of atherosclerosis. Therefore, for the mass transport mechanism, the localized alterations in mass transport (such as oxygen, nucleotide, nitric oxide, low-density lipoproteins (LDL)), especially the accumulation of LDL on the luminal surface would contribute to the localization of atherosclerosis [14,15,23]. Theoretical studies at both the cellular and tissue scale demonstrated that concentration polarization of LDLs, that is LDL concentration increasing from a bulk value towards the interface, occurs in the arterial system and would be enhanced in disturbed blood flow regions [23–29]. Several *in vitro* experiments showed that the lipid concentration polarization was relatively serious in low WSS regions and would affect the accumulation of lipids in the arterial wall [30–33]. However, the correlation of haemodynamics and LDL transport is still ambiguous, since simulations showed that regions with relatively high LDL concentration did not always correspond to low WSS [24,25,34]. Therefore, to reveal the relationship between shear stress and mass transport mechanisms and their roles in atherogenesis, it is necessary to investigate quantitatively the correlation between LDL transport, WSS-based parameters and plaque thickness. To reach this goal, we numerically simulated the blood flow and LDL transport in rabbit aorta and evaluated plaque thickness of the rabbit aorta in several characteristic locations after feeding a high-fat diet. The computational model was obtained from the blood vessel cast using computed tomography (CT). The aortas of the rabbits after feeding a high-fat diet for 10 weeks were stained to study the high incidence areas of atherosclerosis.

2. Material and methods

2.1. Geometric reconstruction of the rabbit aorta

2.1.1. Casting the rabbit arteries

A male white rabbit (15 months and 3.2 kg) was used for the casting procedure. Firstly the rabbit was injected with heparin sodium (approx. 9% w/v) to prevent blood clotting and was then euthanized with an overdose of pentobarbital sodium (100 mg kg^{-1}) via the auricular vein. After carefully opening the abdominal cavity and exposing the heart, two intubation tubes were inserted and ligated into the cardiac left ventricle and cardiac right atrium, respectively. The cannula in the left ventricle was used to rinse the arteries with normal saline, and the blood was flowing out through the cannula in the right atrium at the same time. After quickly flushing the vessels until the colour of the blood was clear, the casting material (self-curing denture acrylic 40 g, methyl methacrylate 50 ml, dimethyl phthalate 20 ml, red pigment 5 g) was infused through the cannula in the left ventricle at a pressure of 100 mmHg [35] until the casting material was hardened and could no longer be injected. Then, the rabbit corpse was left in cold water for 2 days to solidify the casting material fully, and maintained in hydrochloric acid solution (approx. 38% w/v) for two weeks. Finally, the casting vessel was removed from the acid solution and gently washed with detergent solution [36]. The obtained cast of the rabbit arteries is shown in figure 1*a*.

2.1.2. Reconstructing the geometric model of the rabbit aorta

The cast of the rabbit arteries was imaged using a micro-CT scanner (Skyscan1076, v. 2.6, Belgium) with a slice thickness of 0.018 mm, a reconstruction spacing/increment of 0.162 mm, a slice overlap of 0.018 mm and an image resolution of 3876 × 2584. The total number of slices was 3693. The images scanned were segmented by Mimics software (v. 9.0, Materialise, Ann Arbor, MI, USA) to reconstruct the three-dimensional model of the rabbit artery, which was slightly smoothed by Geomagic (v. 2012, Geomagic, North Carolina, USA). Then, the geometric model (figure 1*b*) was meshed using ICEM (ANSYS, Inc., Canonsburg, PA, USA) with a mixture of tetrahedral and prism volume meshes (figure 1*c*) which included 1 379 803 elements. The boundary layer had the element adjacent to the wall of 0.001 mm progressively growing over 15 layers to a total thickness of 0.38 mm. The meshes near the arterial wall were specially refined and the exponential growth was used for the geometric growth to catch the steep variation in flow and mass transport. Mesh independence was considered to be achieved when the averaged difference in WSS and LDL concentration between two successive simulations was less than 1% under steady conditions.

2.1.3. Governing equations

Blood was modelled as a homogeneous and incompressible Newtonian fluid. The arterial wall was assumed to be a no-slip rigid wall [37,38]. The numerical simulation was based on a three-dimensional incompressible Navier–Stokes equation and the conservation of mass:

$$\rho\left[\frac{\partial \boldsymbol{u}}{\partial t} + (\boldsymbol{u}\cdot\nabla)\boldsymbol{u}\right] + \nabla p - \mu\nabla^2\boldsymbol{u} = 0 \tag{2.1}$$

and

$$\nabla\cdot\boldsymbol{u} = 0, \tag{2.2}$$

where ρ and μ is, respectively, the density and viscosity of rabbit blood ($\rho = 1050$ kg m^{-3} and $\mu = 3.5\times10^{-3}$ kg m^{-1} s^{-1}), $\boldsymbol{u}$ and p, respectively, represent the three-dimensional velocity vector field and the pressure field within the rabbit aorta.

Mass transport of LDLs in flowing blood can be described by the following:

$$\frac{\partial c}{\partial t} + \boldsymbol{u}\cdot\nabla c - D\Delta c = 0, \tag{2.3}$$

where c is the concentration of LDLs and D is the diffusion coefficient of LDL in blood, assumed to be 4.8×10^{-12} m^2 s^{-1} [4].

2.1.4. Parameter values

The Schmidt number, which is used to characterize the ratio of movement viscosity coefficient to the diffusion coefficient, is defined as

$$Sc = \frac{\mu}{\rho\cdot D} = \frac{\upsilon}{D}. \tag{2.4}$$

LDL transport is characterized by a high Schmidt number, and the Schmidt number is approximately 6.94×10^5.

The Peclet number, used to indicate the relative proportion of convection to diffusion, is the product of the Reynolds number (*Re*) and Schmidt number (*Sc*). In this study, the time-averaged *Re* was calculated to be approximately 360 (mean flow velocity was 0.199 m s^{-1}, the diameter of the aortic root inflow plane was 6.132×10^{-3} m, measured from the geometry). The Peclet number is approximately 2.49×10^8.

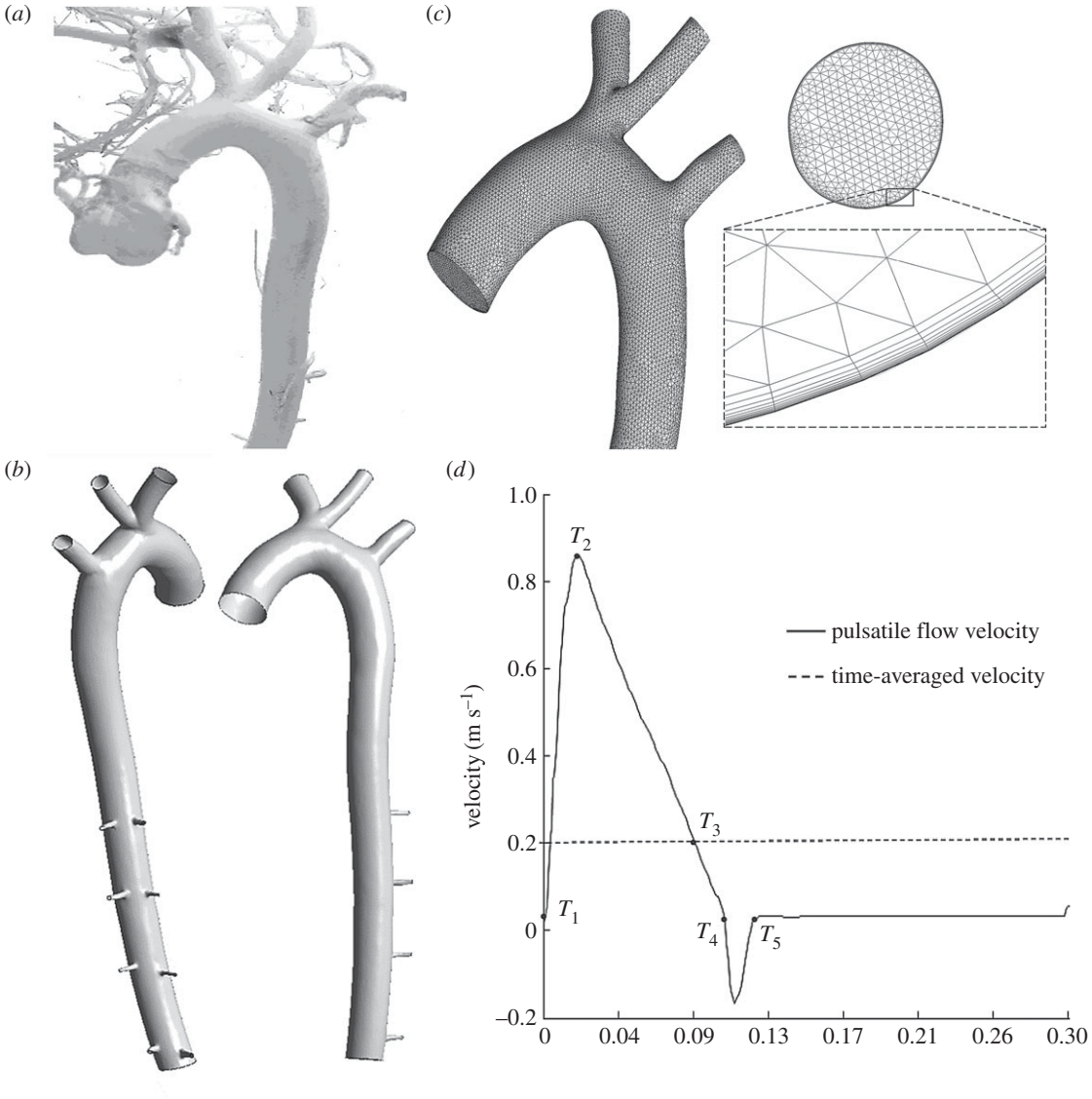

Figure 1. The computational model of the rabbit aortic arch and descending thoracic aorta. (*a*) The cast of the rabbit arteries, (*b*) the geometrical model after trimming, segmenting and smoothing, (*c*) the meshed model of the rabbit aortic arch and inlet. (*d*) The flow waveform at the inlet of the ascending aorta.

Owing to the high Peclet number, the grid near the wall should be quite small and the smallest grid size in the inner wall surfaces, is defined as [39]

$$\Delta r_{\min} = \frac{\delta_C}{3} = \frac{\delta}{3 \cdot \sqrt[3]{Sc}} = \frac{2.28\sqrt{2\nu/\omega}}{3 \cdot \sqrt[3]{Sc}}, \tag{2.5}$$

where δ_C represents the LDL boundary layer thickness, δ represents the boundary layer thickness of the oscillatory flow and ω denotes the angular frequency of the cardiac cycle. The smallest grid size is approximately estimated as 4.84×10^{-3} mm.

2.1.5. Boundary conditions

The simulations were performed under both steady-state flow and pulsatile flow conditions. The inlet flow wave shown in figure 1*d*, was based on experimental measurements [35,40]. The time-averaged *Re* was calculated to be approximately 360 (mean flow velocity was 0.199 m s^{-1}). The outflow condition was used for all outlets. Flow splits into the right common carotid artery and right subclavian artery were 10.9% of the inflow at the aortic root, meanwhile 3.8% went into the left common carotid artery, 7.1% went into the left subclavian artery and 0.156% went into each intercostal branch. The eight intercostal branches, received 1.25% of the inflow at the aortic root [41].

The boundary conditions for mass transport equation were as follows:

$$\text{inlet:} \quad c = c_0, \tag{2.6}$$

$$\text{outlet:} \quad \frac{\partial c_n}{\partial n} = 0, \tag{2.7}$$

and

$$\text{wall:} \quad v_w c_w - D_{\text{LDL}}\left(\frac{\partial c}{\partial n}\right) = 0, \tag{2.8}$$

where v_w is the filtration velocity of LDL across the vessel wall ($v_w = 3.5 \times 10^{-8}$ ms^{-1}) [42], and c_w is the concentration of LDLs at the luminal surface of the artery. The suffix n indicates the direction normal to the boundary.

2.1.6. Computation procedures

A validated finite volume-based algorithm ANSYS Fluent 14.5 (ANSYS, Lebanon, NH, USA) was used for the simulations. A user-defined C-like function was used to solve the mass transport equation of LDL [25,26]. The spatial discretization of the LDL transport used in this study was second-order upwind and the numerical results had been effectively estimated [43,44].

2.1.7. WSS-based haemodynamic indicators

Four WSS-based haemodynamic parameters (time-averaged wall shear stress (TAWSS), OSI, RRT and transWSS) were calculated

through a MATLAB programming environment (The MathWorks, Natick, MA, USA).

The TAWSS, which was used to evaluate the WSS on the vessel wall in pulsatile flow, was defined as follows:

$$\mathrm{TAWSS} = \frac{1}{T}\int_0^T |\mathrm{WSS}(\mathbf{s}, t)| \cdot \mathrm{d}t, \tag{2.9}$$

where T is the duration of the cardiac cycle, WSS is the instantaneous WSS vector and $\mathbf{s}$ is the position on the vessel wall.

The oscillatory shear stress index (OSI), which was often used to measure the directional change of WSS during the cardiac cycle and describe the disturbance of a flow field, was defined as [45]

$$\mathrm{OSI} = 0.5\left[1 - \left(\frac{\left|1/T\int_0^T \mathrm{WSS}(\mathbf{s}, t) \cdot \mathrm{d}t\right|}{1/T\int_0^T |\mathrm{WSS}(\mathbf{s}, t)| \cdot \mathrm{d}t}\right)\right]. \tag{2.10}$$

The RRT introduced to reflect the residence time of particles near the vessel wall, was calculated as [20,46]

$$\mathrm{RRT} = \frac{1}{(1 - 2 \cdot \mathrm{OSI}) \cdot \mathrm{TAWSS}}. \tag{2.11}$$

transWSS was defined as

$$\mathrm{transWSS} = \frac{1}{T}\int_0^T \left|\mathrm{WSS}(\mathbf{s}, t) \cdot \left(n \times \frac{\frac{1}{T}\int_0^T \mathrm{WSS}(\mathbf{s}, t) \cdot \mathrm{d}t}{\left|\frac{1}{T}\int_0^T \mathrm{WSS}(\mathbf{s}, t) \cdot \mathrm{d}t\right|}\right)\right| \cdot \mathrm{d}t, \tag{2.12}$$

where n represents the normal to the arterial surface.

transWSS is to distinguish between uniaxial pulsatile flow and multidirectional flow for capturing multi-directionality [21,22], and it averages over the cardiac cycle the magnitude of those components of the instantaneous WSS vector that are perpendicular to the mean WSS vector in the plane of the endothelium.

2.2. Obtaining the atherosclerotic rabbits and tissues

2.2.1. Atherosclerotic rabbits obtained from a high-fat diet

Four male rabbits were fed with a high-fat diet to get atherosclerotic arteries. The prescription of a high-fat diet includes 2% cholesterol, 10% lard, 0.5% bile salt, 10% egg yolk powder and 77.5% ordinary feed [47,48]. Each rabbit took 150 g food and drank water freely every day. After 10 weeks of feeding, all rabbits were sacrificed to obtain the atherosclerotic aorta.

2.2.2. Haematoxylin and eosin staining of arterial specimen

The aorta and all the branches were fixed with 4% paraformaldehyde for 24 h after being removed from the rabbit and gently washed with saline solution. The tissues were imbedded and numbered according to the routine of paraffin sections, and then sliced to a thickness of 5 µm using a manual rotary microtome (CUT4062, Germany). Then the tissue slices were stained with haematoxylin for 10 min and eosin for 1 min successively, and sealed for preservation. The photos of the tissue slices were segmented by an image analysis system to measure the thickness of the intimal hyperplasia. Excel 2010 was used to deal with the data. All quantitative results were expressed as mean ± s.d.

3. Results

3.1. The low-density lipoprotein concentration distribution on the luminal surface of the aorta

Figure 2*a* shows the distribution of time-averaged LDL concentration (c_w) on the luminal surface of the aorta during the pulsatile cycle. The luminal surface LDL concentration in the ascending aorta was relatively uniform, and 2–4% higher than the bulk LDL concentration (c_0). While the distribution of c_w in the aortic arch and descending aorta was quite uneven with relatively high concentration in the inner side of the arterial wall. Among these regions, the maximum concentration in the aorta was located at the distal end of the aortic arch (Region C), where c_w was 11% higher than c_0. In addition, the luminal surface LDL concentration at the entrance of the brachiocephalic artery (Region A) and the proximal part of the intercostal branch entrance (Region D) was also relatively high, which was 7–8% higher than c_0. And the c_w was slightly higher in the entrance of the left subclavian artery (Region B). However, c_w in the outer wall of the descending aorta (Region E) was as low as most regions of the aorta.

3.2. Wall shear stress-based haemodynamic indicators

Figure 2*b–f* shows WSS distribution within the aorta under the steady flow condition and WSS-based haemodynamic indicators including TAWSS, transWSS, OSI and RRT under pulsatile flow conditions. Generally speaking, regions with low WSS and TAWSS tended to have high OSI, RRT and transWSS. For instance, Region C had the lowest WSS and very low TAWSS as well as quite high OSI and RRT and the highest transWSS. In addition, Regions A and B showed relatively low WSS and TAWSS, which also exhibited slightly high transWSS as well as quite high OSI and RRT. However, the above relationship was not exactly appropriate to Regions D and E. Although the WSS and TAWSS in Region D were quite low, the transWSS was relatively low. Moreover, the WSS and TAWSS were higher in the outer wall of the descending aorta (Region E) than the inner wall of the descending aorta, but the OSI, RRT and transWSS were similar in the two regions.

3.3. Plaque thickness of the specific areas in the rabbit aorta

Figure 3*a*,*b* displays the result of haematoxylin and eosin staining from specific sites of the hypercholesterolaemic rabbit aorta. The specific sites were five regions including Regions A, B, C, D and E. The rabbits formed a typical atherosclerotic plaque after 10 weeks of a high-fat diet, and intimal hyperplasia in the inner surface of the blood vessels increased obviously among Regions A, B, C and D. Nevertheless, there was no lipid deposition or a very small amount of intimal hyperplasia in Region E.

Figure 3*c* demonstrates the quantitative results of plaque thickness. Region C had the thickest intimal hyperplasia, which was up to 365.52 ± 29.36 µm. Regions A and B had the second thickest at 288.23 ± 18.35 µm and 262.85 ± 25.87 µm, respectively. The smallest area was Region D, with only 64.53 ± 6.44 µm ($N = 4$) intimal hyperplasia. No atheromatous plaque formation was observed in Region E.

3.4. The point-by-point correlation among c_w, WSS-based haemodynamic indicators and plaque thickness

The correlation among c_w, WSS-based haemodynamic indicators and atherosclerotic plaque thickness is illustrated in

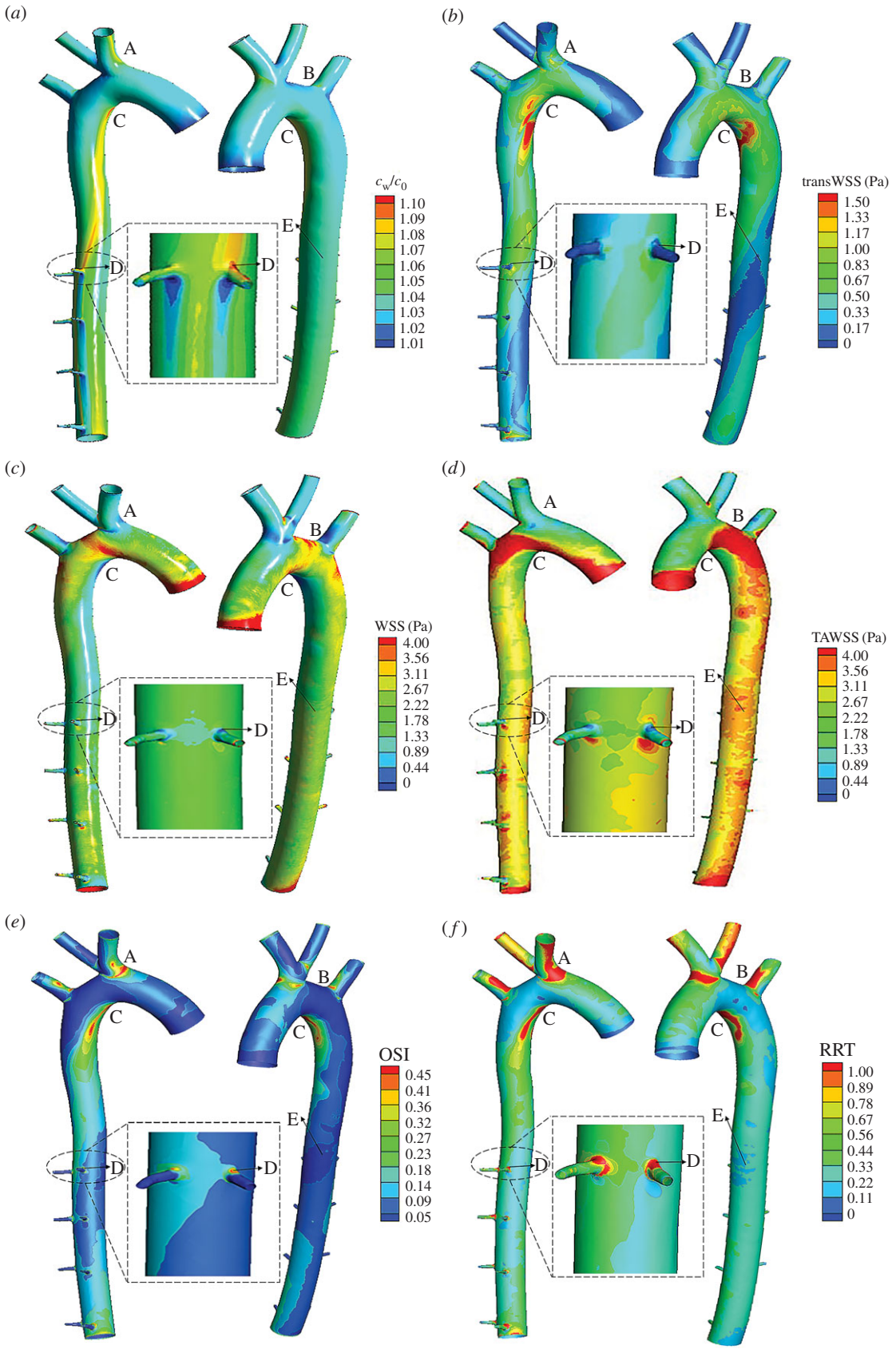

Figure 2. The LDL concentration (c_w) distribution and WSS-based haemodynamic indicators. (*a*) Luminal surface LDL concentration (c_w) distribution, (*b*) transWSS distribution, (*c*) WSS, (*d*) TAWSS distribution, (*e*) oscillatory shear stress index (OSI) and (*f*) RRT distribution.

table 1. Generally speaking, the region with higher plaque thickness was often accompanied by high c_w, OSI, RRT and transWSS, as well as low WSS and TAWSS. Therefore, these regions were more likely to develop atherosclerosis. However, when compared to TAWSS, OSI and RRT, luminal surface LDL concentration and transWSS had a stronger correlation with plaque thickness, where the higher luminal surface LDL concentration and transWSS led to a thicker plaque. Specifically, Region C had the thickest intimal hyperplasia, at the same time, it exhibited the highest c_w and transWSS, lowest WSS, but only quite high OSI and RRT, instead of the highest OSI and RRT. The thickness of intimal

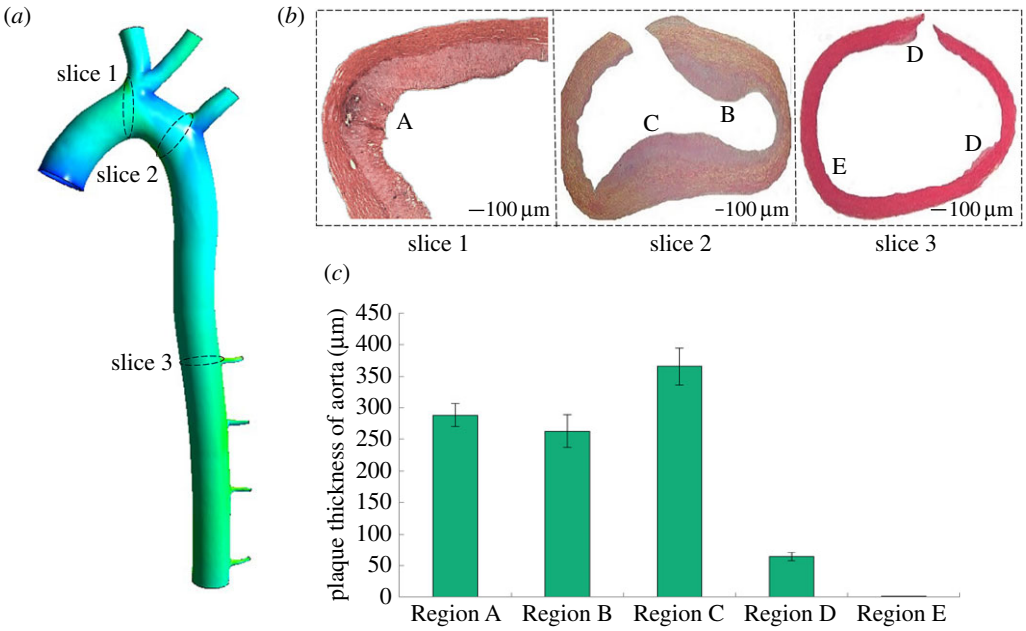

Figure 3. The histological examination and assessment of atherosclerosis in rabbits fed with a high fat diet. (*a*,*b*) Cross section of the aorta tissue specimen stained with haematoxylin and eosin, (*c*) mean plaque thickness of the high-fat diet rabbit aorta (in micrometres).

hyperplasia was comparatively high in Regions A and B where displaying relatively high OSI, slightly high c_w, RRT and transWSS as well as considerably low WSS and TAWSS. However, the above general correlation was not applicable to all regions. Region D only had slight intimal hyperplasia, but had relatively high c_w, OSI and RRT as well as low WSS, TAWSS. In addition, there was no plaque in Region E where the luminal surface LDL concentration, OSI, RRT and transWSS were comparable to most regions in the aorta, but the WSS and TAWSS were higher than most regions. Conclusively, severe intimal hyperplasia corresponded to a high luminal LDL concentration and severely negative haemodynamic environments (HEs) including high OSI, RRT and transWSS, as well as low WSS and TAWSS. Less severe intimal hyperplasia was related to either a moderately high LDL concentration or moderately negative HEs.

4. Discussion

Blood flow-induced shear stress and mass transport have been recognized to play an important role in the development of atherosclerotic localization. To investigate the relationship between the two factors and their roles in the atherogenesis, we numerically simulated blood flow and LDL transport in rabbit aorta and evaluated plaque thickness of the rabbit aorta after feeding a high-fat diet for 10 weeks. The numerical results showed that regions with a high luminal LDL concentration tend to have severely negative HEs including high OSI, RRT and transWSS, as well as low WSS and TAWSS. However, for regions with moderately and slightly high luminal LDL concentration, the relationship between LDL concentration and the above haemodynamic indicators are not clear cut. The experimental results indicated that there is almost no atherosclerotic plaque in regions with both low LDL concentration and positive HEs. In addition, regions with less severe atherosclerotic plaque have either moderately high LDL concentration or moderately negative HEs. Moreover, severe atherosclerotic plaque corresponds to high LDL concentration and seriously negative HEs.

Our numerical study revealed that the luminal surface LDL concentration c_w was higher than the bulk concentration c_0 along the whole aorta and distributed relatively unevenly in the aorta. These results are consistent with previous simulations from simplified arterial models to studies of realistic arteries [49]. Moreover, analytical and experimental results demonstrated that the concentration at the interface of the arterial lumen will directly affect the accumulation of LDLs inside the arterial wall layers [33,50]. Therefore, the enhanced c_w in the rabbit aorta would contribute to the localization of atherosclerosis.

There have been few studies that have comprehensively analysed the relationship between c_w and the WSS-based parameters. Most previous studies have only focused on the relationship between c_w and WSS, [24,25,34,51] and indicated that regions of high LDL concentration in the arteries corresponded to low WSS ones, even in stenosed arteries and at the aorta–iliac bifurcation, [52,53] and c_w not only depends on WSS, [14,15] but also on flow pattern. These results are also demonstrated in our simulations of the rabbit aorta. Moreover, we further investigated other haemodynamic parameters, including TAWSS, OSI, RRT and transWSS in the rabbit aorta and showed that regions with high luminal LDL concentration (Region C) tend to have high OSI, RRT and transWSS, as well as low TAWSS. However, for regions with moderately and slightly high luminal LDL concentrations, the relationship between LDL concentration and the above haemodynamic indicators is not clear cut, where the distribution of LDL concentration and transWSS in the aorta is more similar and scattered when compared with that of OSI and RRT. This phenomenon demonstrated that the blood flow in both the circumferential and axial directions might affect the luminal surface LDL concentration [51].

Based on the simulation results of blood flow and LDL transport, we selected five regions in the rabbit aorta to show the development of the localized atherosclerosis. The flow in the Regions A, B, C and D were very seriously

Table 1. The degree of plaque thickness, luminal surface LDL concentration (c_w) distribution and the WSS-based haemodynamic indicators in Regions A–E. →, the value of most regions of the aorta; ↑/↓, the value is a little higher or lower than that of the most regions; ↑↑/↓↓, the value is obviously higher or lower than that of most regions; ↑↑↑/↓↓↓, the value is particularly higher or lower than that of most regions.

	the degree of c_w, WSS-based haemodynamic indicators and plaque thickness						
	plaque thickness (μm)	LDL concentration	WSS (Pa)	TAWSS (Pa)	OSI	RRT	transWSS (Pa)
Region A	↑↑ (288.23 ± 18.35)	↑↑ (1.07)	↓↓ (0.33)	↓↓ (1.01)	↑↑ (0.47)	↑↑ (16.23)	↑↑ (0.92)
Region B	↑↑ (262.85 ± 25.87)	↑ (1.05)	↓↓ (0.31)	↓↓ (0.96)	↑↑ (0.41)	↑ (6.18)	↑ (0.48)
Region C	↑↑↑ (365.52 ± 29.36)	↑↑↑ (1.11)	↓↓↓ (0.04)	↓↓ (1.47)	↑↑ (0.47)	↑↑ (16.47)	↑↑↑ (2.45)
Region D	↑ (64.53 ± 6.44)	↑↑ (1.08)	↓↓ (0.27)	↓↓↓ (0.34)	↑↑ (0.46)	↑↑ (16.36)	↓ (0.12)
Region E	→ (0)	→ (1.03)	↑ (3.11)	↑ (3.53)	→ (0.04)	→ (0.39)	→ (0.26)

disturbed, conversely the blood in Region E was similar to most areas of the aorta. The experimental results demonstrate that plaque thickness is elevated significantly in the Regions A, B and C, and slightly in Region D, but there was almost no intima hyperplasia in Region E. These predisposed areas of atherosclerosis in the rabbit aorta are consistent with the findings by Rodkiewicz *et al.* [54]. In addition, plaque thickness in the aortic arch (365.52 ± 29.36 μm) is close to the previous histological examination and assessment of atherosclerosis in rabbits fed a similar high-fat diet with 2% cholesterol for 10 weeks (306.70 ± 20.37 μm) [55].

Furthermore, point-by-point comparison between WSS-based haemodynamic indicators and plaque thickness (table 1) shows that there is moderate correlation between plaque thickness and TAWSS, OSI as well as RRT. These results are consistent with the previous systematic review about the relationship between these metrics and intimal, intima–medial or wall thickness [34], but incompatible with many previous studies [56]. By contrast, luminal surface LDL concentration and transWSS have a relatively strong correlation with plaque thickness, where the higher luminal surface LDL concentration and transWSS lead to a thicker plaque. However, there is still an exception. For instance, plaque thickness at Region D was not particularly high, but it had a relatively high LDL concentration, and transWSS was even lower instead of being increased. This may be partly explained by the process of LDL infiltration into the vessel wall. The uptake of LDL in the arteries is determined by both LDL concentration polarization [57] and the permeability of endothelial cells to LDLs. It is well documented that haemodynamic factors would affect the function of endothelial cells and hence the permeability [58,59]. It has been perceived that the degree of concentration polarization would increase if the transmural water flux velocity was increased [30,31]. Therefore, plaque thickness may be determined by the synergetic effects of the luminal surface LDL concentration and WSS-based haemodynamic indicators.

The present study had some limitations. Firstly, the model was obtained using casting technology, which would slightly damage the geometry of the aorta. However, studies using human aorta models constructed based on *in vivo* MRI slices have shown similar results [25]. Secondly, numerical simulations were influenced. Some assumptions were used in this simulation, including Newtonian blood fluid, rigid artery walls, wall-free model and inlet boundary conditions. For the Newtonian fluid assumption, Iasiello *et al.* [53] believed the Newtonian fluid assumption could still be considered reliable for medium and large arteries. Our group has previously obtained similar results [25] and the Newtonian fluid assumption can approximate the distribution of LDL. For the rigid wall assumption, a previous study [60] showed a rigid wall, which lacked wall movement, should have influence on local blood flow and hence on LDL transport. For the wall-free model, the analysis is restricted within the lumen and the LDL transport to the wall is treated as a simple boundary condition. This model can basically be used to investigate the influence of haemodynamics on LDL concentration distribution [49,51,61–64], but it is unable to provide the transport process of LDL in the blood vessel walls. For the inlet boundary condition, it is quite hard to obtain a precise profile due to the highly complex flow situation as well as the individual differences in anatomy, but in comparison with the *in vivo* data [65], this assumption may only affect the accuracy of the prediction on the absolute value of our results, instead of the main haemodynamic features. Thirdly, we manually chose point-by-point comparison to be as accurate as possible, but there were errors due to the influence of human differences, and finding a more accurate algorithm to match areas automatically is the goal of our future efforts. Lastly, the geometry of the blood vessel would change when the plaque thickness formed, and it would influence the haemodynamic conditions and LDL transport to a certain extent [66,67]. Therefore, to better understand the mechanism of atherosclerosis, a detailed and holistic understanding of blood flow and mass transport within the rabbit aorta should be considered under more realistic geometry and simulation conditions in the future. In particular, future studies should investigate the effects of a realistic inflow velocity profile at the aortic root and the complex biological and chemical processes involved in atherogenesis.

5. Conclusion

In this study, the relationship between haemodynamic indicators and mass transport and their roles in atherosclerosis in the rabbit aortic arch and descending thoracic aorta are investigated. Severe atherosclerotic plaque corresponds to a high LDL concentration and seriously negative HEs. Less severe atherosclerotic plaque is related to either moderately high LDL concentrations or moderately negative HEs. There was almost no atherosclerotic plaque in regions with both low LDL concentration and positive HEs. Therefore, the synergetic effects of luminal surface LDL concentration and

haemodynamic factors may determine plaque thickness and contribute to localized atherosclerosis.

Authors' contributions. X.L. and X.L. participated in the design of the study and drafted the manuscript; P.Z. carried out the statistical analyses; C.F. helped to determine the geometry; A.S., H.K., X.D. and Y.F. coordinated the study and helped draft the manuscript. All authors gave final approval for publication.

Competing interests. We have no competing interests.

Funding. This work was supported by the National Natural Science Research Foundation of China Grants-in-Aid (grant nos. 11572028, 61190123, 31570947, 11421202, 61533016 and 11572029), National key research and development programme in China (grant no. 2016YFC1102202 and 2016YFC1101100), Special Fund for Excellent Doctor Degree Dissertation of Beijing (20131000601) and the 111 Project (B13003).

Acknowledgements. The authors would like to thank Zhenmin Fan and Xiaopeng Tian for assisting in modelling.

References

1. Debakey ME, Lawrie GM, Glaeser DH. 1985 Patterns of atherosclerosis and their surgical significance. *Ann. Surg*. **201**, 115–131. (doi:10.1097/00000658-198502000-00001)
2. Spain DM. 1966 Atherosclerosis. *Sci. Am*. **215**, 48–56. (doi:10.1038/scientificamerican0866-48)
3. Kwak BR *et al.* 2014 Biomechanical factors in atherosclerosis: mechanisms and clinical implications. *Eur. Heart J*. **35**, 3013–3020. (doi:10.1093/eurheartj/ehu353)
4. Caro CG, Fitzgerald JM, Schroter RC. 1971 Atheroma and arterial wall shear observation, correlation and proposal of a shear dependent mass transfer mechanism for atherogenesis. *Proc. R. Soc. Lond. B* **177**, 109–159. (doi:10.1098/rspb.1971.0019)
5. Malek AM, Alper SL, Izumo S. 1999 Hemodynamic shear stress and its role in atherosclerosis. *JAMA* **115**, 2035–2042. (doi:10.1001/jama.282.21.2035)
6. Chiu JJ, Chien S. 2011 Effects of disturbed flow on vascular endothelium: pathophysiological basis and clinical perspectives. *Physiol. Rev*. **91**, 327–387. (doi:10.1152/physrev.00047.2009)
7. Ethier CR. 2002 Computational modeling of mass transfer and links to atherosclerosis. *Ann. Biomed. Eng*. **30**, 461–471. (doi:10.1114/1.1468890)
8. Khakpour M, Vafai K. 2008 Critical assessment of arterial transport models. *Int. J. Heat Mass Transf*. **51**, 807–822. (doi:10.1016/j.ijheatmasstransfer.2007.04.021)
9. Choi HW, Ferrara KW, Barakat AI. 2007 Modulation of ATP/ADP concentration at the endothelial surface by shear stress: effect of flow recirculation. *Ann. Biomed. Eng*. **35**, 505–516. (doi:10.1007/s10439-006-9247-9)
10. Liu X, Fan Y, Sun A, Deng X. 2013 Numerical simulation of nucleotide transport in the human thoracic aorta. *J. Biomech*. **46**, 819–827. (doi:10.1016/j.jbiomech.2012.11.009)
11. Xiao L, Yubo F, Xiaoyan D. 2010 Effect of spiral flow on the transport of oxygen in the aorta: a numerical study. *Ann. Biomed. Eng*. **38**, 917–926. (doi:10.1007/s10439-009-9878-8)
12. Liu X, Fan Y, Xu XY, Deng X. 2012 Nitric oxide transport in an axisymmetric stenosis. *J. R. Soc. Interface* **9**, 2468–2478. (doi:10.1098/rsif.2012.0224)
13. Liu X, Wang Z, Zhao P, Fan Z, Sun A, Zhan F, Fan Y, Deng X. 1932 Nitric oxide transport in normal human thoracic aorta: effects of hemodynamics and nitric oxide scavengers. *PLoS ONE* **9**, e112395. (doi:10.1371/journal.pone.0112395)
14. Comerford A, David T. 2008 Computer model of nucleotide transport in a realistic porcine aortic trifurcation. *Ann. Biomed. Eng*. **36**, 1175–1187. (doi:10.1007/s10439-008-9493-0)
15. Cantwell CD *et al.* 2015 Nektar++: an open-source spectral/hp element framework. *Comput. Phys. Commun*. **192**, 205–219. (doi:10.1016/j.cpc.2015.02.008)
16. Dai G, Kaazempur-Mofrad MR, Natarajan S, Zhang Y, Vaughn S, Blackman BR, Kamm RD, Garcia-Cardena G, Gimbrone MA. 2004 Distinct endothelial phenotypes evoked by arterial waveforms derived from atherosclerosis-susceptible and -resistant regions of human vasculature. *Proc. Natl Acad. Sci. USA* **101**, 14 871–14 876. (doi:10.1073/pnas.0406073101)
17. Li Y-SJ, Haga JH, Chien S. 2005 Molecular basis of the effects of shear stress on vascular endothelial cells. *J. Biomech*. **38**, 1949–1971. (doi:10.1016/j.jbiomech.2004.09.030)
18. Chien S. 2003 Molecular and mechanical bases of focal lipid accumulation in arterial wall. *Prog. Biophys. Mol. Biol*. **83**, 131–151. (doi:10.1016/S0079-6107(03)00053-1)
19. He X, Ku DN. 1996 Pulsatile flow in the human left coronary artery bifurcation: average conditions. *J. Biomech. Eng*. **118**, 74–82. (doi:10.1115/1.2795948)
20. Himburg HA, Grzybowski DM, Hazel AL, Lamack JA, Li XM, Friedman MH. 2004 Spatial comparison between wall shear stress measures and porcine arterial endothelial permeability. *AJP Heart Circul. Physiol*. **286**, H1916–H1922. (doi:10.1152/ajpheart.00897.2003)
21. Peiffer V, Sherwin SJ, Weinberg PD. 2013 Computation in the rabbit aorta of a new metric—the transverse wall shear stress—to quantify the multidirectional character of disturbed blood flow. *J. Biomech*. **46**, 2651–2658. (doi:10.1016/j.jbiomech.2013.08.003)
22. Mohamied Y, Rowland EM, Bailey EL, Sherwin SJ, Schwartz MA, Weinberg PD. 2015 Change of direction in the biomechanics of atherosclerosis. *Ann. Biomed. Eng*. **43**, 16–25. (doi:10.1007/s10439-014-1095-4)
23. Deng X, Marois Y, How T, Merhi Y, King M, Guidoin R. 1995 Luminal surface concentration of lipoprotein (LDL) and its effect on the wall uptake of cholesterol by canine carotid arteries. *J. Vasc. Surg*. **21**, 135–145. (doi:10.1016/S0741-5214(95)70252-0)
24. Wada S, Karino T. 2002 Theoretical prediction of low-density lipoproteins concentration at the luminal surface of an artery with a multiple bend. *Ann. Biomed. Eng*. **30**, 778–791. (doi:10.1114/1.1495868)
25. Liu X, Pu F, Fan Y, Deng X, Li D, Li S. 2009 A numerical study on the flow of blood and the transport of LDL in the human aorta: the physiological significance of the helical flow in the aortic arch. *Am. J. Physiol. Heart Circul. Physiol*. **297**, H163–H170. (doi:10.1152/ajpheart.00266.2009)
26. Liu X, Fan Y, Deng X, Zhan F. 2011 Effect of non-Newtonian and pulsatile blood flow on mass transport in the human aorta. *J. Biomech*. **44**, 1123–1131. (doi:10.1016/j.jbiomech.2011.01.024)
27. Vincent PE, Sherwin SJ, Weinberg PD. 2010 The effect of the endothelial glycocalyx layer on concentration polarisation of low density lipoprotein in arteries. *J. Theor. Biol*. **265**, 1–17. (doi:10.1016/j.jtbi.2010.04.015)
28. Vincent PE, Sherwin SJ, Weinberg PD. 2009 The effect of a spatially heterogeneous transmural water flux on concentration polarization of low density lipoprotein in arteries. *Biophys. J*. **96**, 3102–3115. (doi:10.1016/j.bpj.2009.01.022)
29. Liu X, Fan Y, Deng X. 2011 Effect of the endothelial glycocalyx layer on arterial LDL transport under normal and high pressure. *J. Theor. Biol*. **283**, 71–81. (doi:10.1016/j.jtbi.2011.05.030)
30. Wang G, Deng X, Guidoin R. 2003 Concentration polarization of macromolecules in canine carotid arteries and its implication for the localization of atherogenesis. *J. Biomech*. **36**, 45–51. (doi:10.1016/S0021-9290(02)00277-4)
31. Zhang ZG, Deng XY. 2007 *Ex vitro* experimental study on concentration polarization of macromolecules (LDL) at an arterial stenosis. *Sci. China* **50**, 486–491. (doi:10.1007/s11427-007-0068-3)
32. Ding Z, Fan YX, Sun A, Kang H. 2010 3,3′-Dioctadecylindocarbocyanine-low-density lipoprotein uptake and flow patterns in the rabbit aorta–iliac bifurcation under three perfusion flow conditions. *Exp. Biol. Med*. **235**, 1062–1071. (doi:10.1258/ebm.2010.010035)
33. Zhenze W, Xiao L, Hongyan K, Anqiang S, Yubo F, Xiaoyan D. 2014 Enhanced accumulation of LDLs within the venous graft wall induced by elevated filtration rate may account for its accelerated atherogenesis. *Atherosclerosis* **236**, 198–206. (doi:10.1016/j.atherosclerosis.2014.07.006)

34. Lantz J, Karlsson M. 2012 Large eddy simulation of LDL surface concentration in a subject specific human aorta. *J. Biomech*. **45**, 537–542. (doi:10.1016/j.jbiomech.2011.11.039)
35. Avolio AP, O'Rourke MF, Mang K, Bason PT, Gow BS. 1976 A comparative study of pulsatile arterial hemodynamics in rabbits and guinea pigs. *Am. J. Physiol*. **230**, 868–875.
36. Vincent PE, Plata AM, Hunt AA, Weinberg PD, Sherwin SJ. 2011 Blood flow in the rabbit aortic arch and descending thoracic aorta. *J. R. Soc. Interface* **8**, 1708–1719. (doi:10.1098/rsif.2011.0116)
37. Friedman MH, Bargeron CB, Duncan DD, Hutchins GM, Mark FF. 1992 Effects of arterial compliance and non-Newtonian rheology on correlations between intimal thickness and wall shear. *J. Biomech. Eng*. **114**, 317–320. (doi:10.1115/1.2891383)
38. Jr MJ, Maier SE, Ku DN, Boesiger P. 1994 Hemodynamics in the abdominal aorta: a comparison of *in vitro* and *in vivo* measurements. *J. Appl. Physiol*. **76**, 1520.
39. Tada S. 2010 Numerical study of oxygen transport in a carotid bifurcation. *Phys. Med. Biol*. **55**, 3993. (doi:10.1088/0031-9155/55/14/004)
40. Alastruey J, Nagel SR, Nier BA, Hunt AAE, Weinberg PD, Peiró J. 2009 Modelling pulse wave propagation in the rabbit systemic circulation to assess the effects of altered nitric oxide synthesis. *J. Biomech*. **42**, 2116–2123. (doi:10.1016/j.jbiomech.2009.05.028)
41. Barakat AI, Marini RP, Colton CK. 1997 Measurement of flow rates through aortic branches in the anesthetized rabbit. *Lab. Anim. Sci*. **47**, 184–189.
42. Baldwin AL, Wilson LM, Simon BR. 1992 Effect of pressure on aortic hydraulic conductance. *Arterioscl. Thromb. J. Vasc. Biol*. **12**, 163–171. (doi:10.1161/01.ATV.12.2.163)
43. Bird BRB, Stewart WE, Edwi NL. 1958 *Notes on transport phenomena*. New York, NY: John Wiley.
44. Vincent PE, Weinberg PD. 2014 Flow-dependent concentration polarization and the endothelial glycocalyx layer: multi-scale aspects of arterial mass transport and their implications for atherosclerosis. *Biomech. Model. Mechanobiol*. **13**, 313–326. (doi:10.1007/s10237-013-0512-1)
45. Ku DN, Giddens DP, Zarins CK, Glagov S. 1985 Pulsatile flow and atherosclerosis in the human carotid bifurcation. Positive correlation between plaque location and low oscillating shear stress. *Arteriosclerosis* **5**, 293–302. (doi:10.1161/01.ATV.5.3.293)
46. Lee SW, Antiga L, Steinman DA. 2009 Correlations among indicators of disturbed flow at the normal carotid bifurcation. *J. Biomech. Eng*. **131**, 309–321. (doi:10.1115/1.3127252)
47. Kritchevsky D, Tepper SA. 1968 Experimental atherosclerosis in rabbits fed cholesterol-free diets: influence of chow components. *J. Atheroscl. Res*. **8**, 357–369. (doi:10.1016/S0368-1319(68)80070-5)
48. Yang J, Yue ZH, Xie T. 2014 Establishment of atherosclerosis model induced by feeding high-fat diet plus abdominal aorta balloon injury in rabbits. *J. Emerg. Trad. Chin. Med*. **31**, 406–413.
49. Yang N, Vafai K. 2006 Modeling of low-density lipoprotein (LDL) transport in the artery—effects of hypertension. *Int. J. Heat Mass Transfer* **49**, 850–867. (doi:10.1016/j.ijheatmasstransfer.2005.09.019)
50. Kenjereš S, Loor AD. 2014 Modelling and simulation of low-density lipoprotein transport through multi-layered wall of an anatomically realistic carotid artery bifurcation. *J. R. Soc. Interface* **11**, 20130941. (doi:10.1098/rsif.2013.0941)
51. Wang S, Vafai K. 2015 Analysis of low density lipoprotein (LDL) transport within a curved artery. *Ann. Biomed. Eng*. **43**, 1571–1584. (doi:10.1007/s10439-014-1219-x)
52. Nematollahi A, Shirani E, Mirzaee I, Sadeghi MR. 2012 Numerical simulation of LDL particles mass transport in human carotid artery under steady state conditions. *Sci. Iranica* **19**, 519–524. (doi:10.1016/j.scient.2012.03.005)
53. Iasiello M, Vafai K, Andreozzi A, Bianco N. 2016 Analysis of non-Newtonian effects on low-density lipoprotein accumulation in an artery. *J. Biomech*. **49**, 1437–1446. (doi:10.1016/j.jbiomech.2016.03.017)
54. Rodkiewicz CM. 1975 Localization of early atherosclerotic lesions in the aortic arch in the light of fluid flow. *J. Biomech*. **8**, 149–156. (doi:10.1016/0021-9290(75)90096-2)
55. Zulkhairi A, Hasnah B, Zaiton Z, Jamaludin M, Zanariyah A, Khairul KAK, Tauflk HM. 2006 Atheromatous plaque formation in rabbit aorta fed with high cholesterol diet. *Mal. J. Nutr*. **12**, 213–220.
56. Veronique P, Sherwin SJ, Weinberg PD. 2013 Does low and oscillatory wall shear stress correlate spatially with early atherosclerosis? A systematic review. *Cardiovasc. Res*. **99**, 242–250.
57. Ding Z, Liu S, Yang B, Fan Y, Deng X. 2012 Effect of oxidized low-density lipoprotein concentration polarization on human smooth muscle cells' proliferation, cycle, apoptosis and oxidized low-density lipoprotein uptake. *J. R. Soc. Interface* **9**, 1233–1240. (doi:10.1098/rsif.2011.0436)
58. Tarbell JM. 2010 Shear stress and the endothelial transport barrier. *Cardiovasc. Res*. **87**, 320–330. (doi:10.1093/cvr/cvq146)
59. Chooi KY, Comerford A, Sherwin SJ, Weinberg PD. 2016 Intimal and medial contributions to the hydraulic resistance of the arterial wall at different pressures: a combined computational and experimental study. *J. R. Soc. Interface* **13**, 20160234. (doi:10.1098/rsif.2016.0234)
60. Jin S, Oshinski J, Giddens DP. 2003 Effects of wall motion and compliance on flow patterns in the ascending aorta. *J. Biomech. Eng*. **125**, 347. (doi:10.1115/1.1574332)
61. Prosi M, Zunino P, Perktold K, Quarteroni A. 2005 Mathematical and numerical models for transfer of low-density lipoproteins through the arterial walls: a new methodology for the model set up with applications to the study of disturbed lumenal flow. *J. Biomech*. **38**, 903–917. (doi:10.1016/j.jbiomech.2004.04.024)
62. Ai L, Vafai K. 2006 A coupling model for macromolecule transport in a stenosed arterial wall. *Int. J. Heat Mass Transfer* **49**, 1568–1591. (doi:10.1016/j.ijheatmasstransfer.2005.10.041)
63. Khakpour M, Vafai K. 2008 A comprehensive analytical solution of macromolecular transport within an artery. *Int. J. Heat Mass Transfer* **51**, 2905–2913. (doi:10.1016/j.ijheatmasstransfer.2007.09.019)
64. Iasiello M, Vafai K, Andreozzi A, Bianco N. 2016 Low-density lipoprotein transport through an arterial wall under hyperthermia and hypertension conditions—an analytical solution. *J. Biomech*. **49**, 193–204. (doi:10.1016/j.jbiomech.2015.12.015)
65. Morbiducci U, Ponzini R, Gallo D, Bignardi C, Rizzo G. 2013 Inflow boundary conditions for image-based computational hemodynamics: impact of idealized versus measured velocity profiles in the human aorta. *J. Biomech*. **46**, 102. (doi:10.1016/j.jbiomech.2012.10.012)
66. Chung S, Vafai K. 2013 Low-density lipoprotein transport within a multi-layered arterial wall—effect of the atherosclerotic plaque/stenosis. *J. Biomech*. **46**, 574–585. (doi:10.1016/j.jbiomech.2012.09.022)
67. Iasiello M, Vafai K, Andreozzi A, Bianco N, Tavakkoli F. 2015 Effects of external and internal hyperthermia on LDL transport and accumulation within an arterial wall in the presence of a stenosis. *Ann. Biomed. Eng*. **43**, 1585–1599. (doi:10.1007/s10439-014-1196-0)